Real-Time Estimation of Intrinsic and Reflex Stiffness

Daniel Ludvig*, *Student Member, IEEE*, and Robert E. Kearney, *Fellow, IEEE*

***Abstract*—Joint stiffness defines the dynamic relationship between the position of the joint and the torque acting about it. Joint stiffness is composed of two components: intrinsic and reflex stiffness. Separating the two stiffness components is difficult because they appear and change together. A number of approaches have been used to distinguish the components, but all these are inherently off-line. We have developed a novel algorithm that estimates the two components of ankle stiffness in real time. Cross-correlations between torque and position, velocity, and acceleration are used to estimate intrinsic stiffness. The reflex torque is then estimated by subtracting the estimated intrinsic components and the reflex stiffness estimated by computing the impulse response function (IRF) between the estimated reflex torque and the half-wave rectified velocity. A novel position perturbation, consisting of pseudo-random pulses of different lengths, is used to eliminate covariance between intrinsic and reflex stiffness estimates. Simulation results showed that the algorithm estimates intrinsic and reflex stiffness very accurately and responds to changes in stiffness in less than 15 s. Validation with experimental data showed that the real-time estimates were in close agreement with the estimates generated by an established off-line intrinsic and reflex stiffness identification algorithm.**

***Index Terms*—Biological control systems, biological motor systems, biomechanics, identification.**

I. Introduction

JOINT stiffness defines the dynamic relationship between the position of the joint and the torque acting about it [1], and consequently it plays an important role in the control of posture in the face of perturbations. It is also vital in the control of movement, since it is the torque produced by the muscles that controls the final joint position. Joint stiffness is composed of two components: intrinsic stiffness, which is generated by the viscoelastic properties of the joint, muscles and connective tissue; and reflex stiffness, which is generated by active muscle contraction in response to the stretch of a muscle.

Although much is known about the two stiffness pathways, measuring each component separately is challenging because intrinsic and reflex stiffness appear and change together. To overcome this, some studies have measured the mechanical properties of the joint before and after elimination of the reflex by deafferenting [2], applying a neural block to [3] or electrically stimulating [4], [5] the primary afferents.

Manuscript received September 11, 2006. This work was supported by the Canadian Institutes of Health Research and the McGill Faculty of Medicine. This work was presented in part at the IEEE EMBS Conference 2006, New York. *Asterisk indicates corresponding author.*

*D. Ludvig is with the Department of Biomedical Engineering, McGill University, Montreal, QC H3A 2B4 Canada (e-mail: daniel.ludvig@mail.mcgill.ca).

R. E. Kearney is with the Department of Biomedical Engineering, McGill University, Montreal, QC H3A 2B4 Canada (e-mail: robert.kearney@mcgill.ca).

Digital Object Identifier 10.1109/TBME.2007.894737

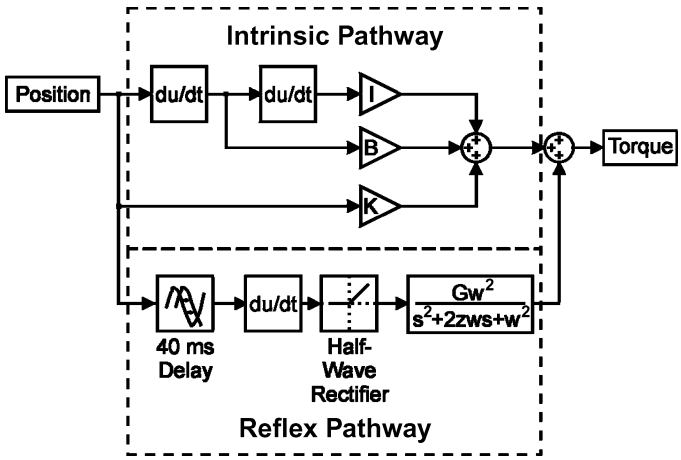

Fig. 1. Intrinsic and reflex components of total joint stiffness. Intrinsic pathway is composed of three components: inertial, viscous and elastic; reflex pathway consists of a differentiator followed by a Hammerstein system where the nonlinearity is a half-wave rectifier and the linearity is a second order low-pass system with a delay.

Another approach is to separate the intrinsic and reflex components analytically. Our laboratory uses a parallel-cascade identification algorithm [6]–[8] to separate intrinsic and reflex stiffness at the ankle. This algorithm separates the two components by modeling the system as two parallel pathways (Fig. 1). The intrinsic pathway has three components: inertial, viscous, and elastic, which are proportional to the joint acceleration, velocity, and position, respectively. The reflex pathway is modeled as a differentiator followed by a Hammerstein system. The nonlinearity has been shown to closely resemble a half-wave rectifier, while the linear element has been modeled as a second or third order low-pass system with a delay of about 40 ms [6], [7]. This algorithm takes advantage of the reflex delay, to estimate intrinsic components independently of the reflex components. The reflex components are estimated once the intrinsic components have been removed and the algorithm repeats the procedure until the estimates converge. Zhang and Rymer [9] used mathematical modeling to estimate intrinsic and reflex components of joint stiffness at the knee. They formulated a nonlinear delay differential equation describing reflex stiffness, and numerically integrated the equation to solve it. Another method estimated the components of the intrinsic stiffness at the ankle by measuring the phase lag as a function of the frequency of the torque, given sinusoidal perturbations [10], [11].

It has been postulated that reflex stiffness can be varied in a task-dependent manner independent of intrinsic stiffness [12]. While studies have shown that intrinsic and reflex stiffness vary in a task-dependent manner, whether they can be voluntarily modulated remains unknown. Voluntary modulation of intrinsic and reflex stiffness would be greatly aided by real-time feedback of intrinsic and reflex stiffness values, which until now

has not been possible. Therefore, an algorithm which could estimate intrinsic and reflex stiffness in real time would permit these estimates to be provided to the subject as feedback.

However, all existing methods are inherently off-line in nature and cannot be used in real time. Therefore, a novel algorithm is needed to estimate reflex and intrinsic stiffness separately in real time. Such an algorithm must:

1) estimate reflex and intrinsic stiffness independently;
2) rely on short segments of data to provide subjects with feedback of current stiffness estimates;
3) be computationally efficient, so that the calculation can be performed in real time.

We have achieved this under stationary conditions at the ankle using the zero lag cross-correlation between position, its derivatives, and torque to estimate the intrinsic stiffness. The impulse response function (IRF) between a half-wave rectified velocity signal and residual torque is used to estimate the reflex stiffness.

The paper is developed as follows. Section II describes the theory underlying the real-time estimation of reflex and intrinsic stiffness and develops estimators for the reflex and intrinsic stiffness. Section III presents the results of a simulation study that demonstrates that the method yields elastic stiffness and reflex stiffness gain estimates which are proportional to the underlying values, do not covary, and documents the response time of the estimates. Section IV presents the results of the experimental validation of the method that demonstrates that the new method produces estimates that are consistent with those obtained with previously validated, off-line methods. Section V discusses the results, suggests ways the methods might be used, and describes areas for future work. A part of this work has been presented at the IEEE EMBS Conference 2006 [13].

II. Real-Time Estimation Algorithm

A. Separation of Intrinsic and Reflex Stiffness

Torque produced at the ankle in response to perturbations arises from three sources: voluntary, intrinsic, and reflex. This can be expressed as

$$TQ = TQ_V + TQ_I + TQ_R \tag{1}$$

where

TQ_V = voluntary torque;
TQ_I = intrinsic torque;
TQ_R = reflex torque.

Thus, the cross-correlation between position and torque is given by

$$E[\theta \bullet TQ] = E[\theta \bullet TQ_V] + E[\theta \bullet TQ_I] + E[\theta \bullet TQ_R]. \tag{2}$$

To use this relation to estimate intrinsic stiffness, it is first necessary to eliminate the voluntary and reflex contributions. If the subject maintains a constant voluntary torque, its contribution can be eliminated by high-pass filtering, thus removing the first term in (2). The high-pass filter must be chosen to eliminate only constant torques; hence, a filter with a low cut-off frequency is used. However, if the cut-off frequency is too low, the algorithm will respond too slowly to changes in the mean torque. We examined this empirically and found that the highest cut-off frequency that did not distort the signal greatly was 0.033 Hz.

Eliminating the reflex contribution to (2) is more complex. Reflex stiffness at the ankle has been modeled as a uni-directional rate-sensitive element followed by a low-pass filter and a delay [6]. Thus, the zero-lag cross-correlation between position and reflex torque can be expressed as

$$E[\theta(t) \bullet TQ_R(t)] = E\left[\theta(t) \bullet \dot{\theta}^+(t) * \mathbf{h}\right] \tag{3}$$

where $\dot{\theta}^+$ is the half-wave rectified velocity, $\mathbf{h}$ is the IRF between $\dot{\theta}^+$ and TQ_R, and t is time. Expanding the convolution as a discrete sum gives

$$E[\theta(t) \bullet TQ_R(t)] = E\Big[\theta(j\Delta t) \bullet \Big(\dot{\theta}^+(j\Delta t)h(0) + \dot{\theta}^+((j-1)\Delta t)h(1) + \cdots + \dot{\theta}^+((j-n)\Delta t)h(n)\Big)\Big] \tag{4}$$

where j is the jth sample, Δt is the sampling increment, and $h(i)$ is the ith element of $\mathbf{h}$. Since $h(i)$ for any given i is constant, it can be taken out of the expectation value and (4) can be rewritten as

$$\begin{aligned} E[\theta(t) \bullet TQ_R(t)] = {} & E\Big[\theta(j\Delta t) \bullet \dot{\theta}^+(j\Delta t)\Big]h(0) \\ & + E\Big[\theta(j\Delta t) \bullet \dot{\theta}^+((j-1)\Delta t)\Big]h(1) + \ldots \\ & + E\Big[\theta(j\Delta t) \bullet \dot{\theta}^+((j-n)\Delta t)\Big]h(n). \end{aligned} \tag{5}$$

Equation (5) can be rewritten in summation notation as follows:

$$E[\theta(t) \bullet TQ_R(t)] = \sum_{i=0}^{n} E\left[\theta(j\Delta t) \bullet \dot{\theta}^+((j-i)\Delta t)\right] h(i). \tag{6}$$

The expectation value in (6) is the cross-correlation between position and half-wave rectified velocity. Thus, the cross-correlation between position and reflex torque is equivalent to

$$E[\theta(t) \bullet TQ_R(t)] = \sum_{i=0}^{n} \Phi_{\theta\dot{\theta}^+}(i)h(i) \tag{7}$$

where $\Phi_{\theta\dot{\theta}^+}(i)$ is the ith lag cross-correlation between position and half-wave rectified velocity.

Using a typical reflex stiffness IRF [Fig. 2(b)] found in [6] and [7], we can determine for any given perturbation whether or not the cross-correlation between position and reflex torque will equal zero by finding $\Phi_{\theta\dot{\theta}^+}$. Fig. 2(a) shows a pseudo-random binary sequence (PRBS) with a 125 ms switching interval, a perturbation signal which has been used to identify intrinsic and reflex stiffness in previous work [6]–[8]. This input has enough power to permit stiffness to be identified while at the same time has a low enough average velocity to preserve the reflex response. The product of the reflex stiffness IRF $(\mathbf{h})$ [Fig. 2(b)] and $\Phi_{\theta\dot{\theta}^+}$ [Fig. 2(c)] for this perturbation is shown in Fig. 2(d) and clearly will not sum to zero, thus cannot be used for the real-time identification. This is because $\mathbf{h}$ is nonzero between 40 and 400 ms, while $\Phi_{\theta\dot{\theta}^+}$ is nonzero for the first 125 ms. To solve this problem, a PRBS with a switching rate of 40 ms could be used; however, previous experiments have shown that high

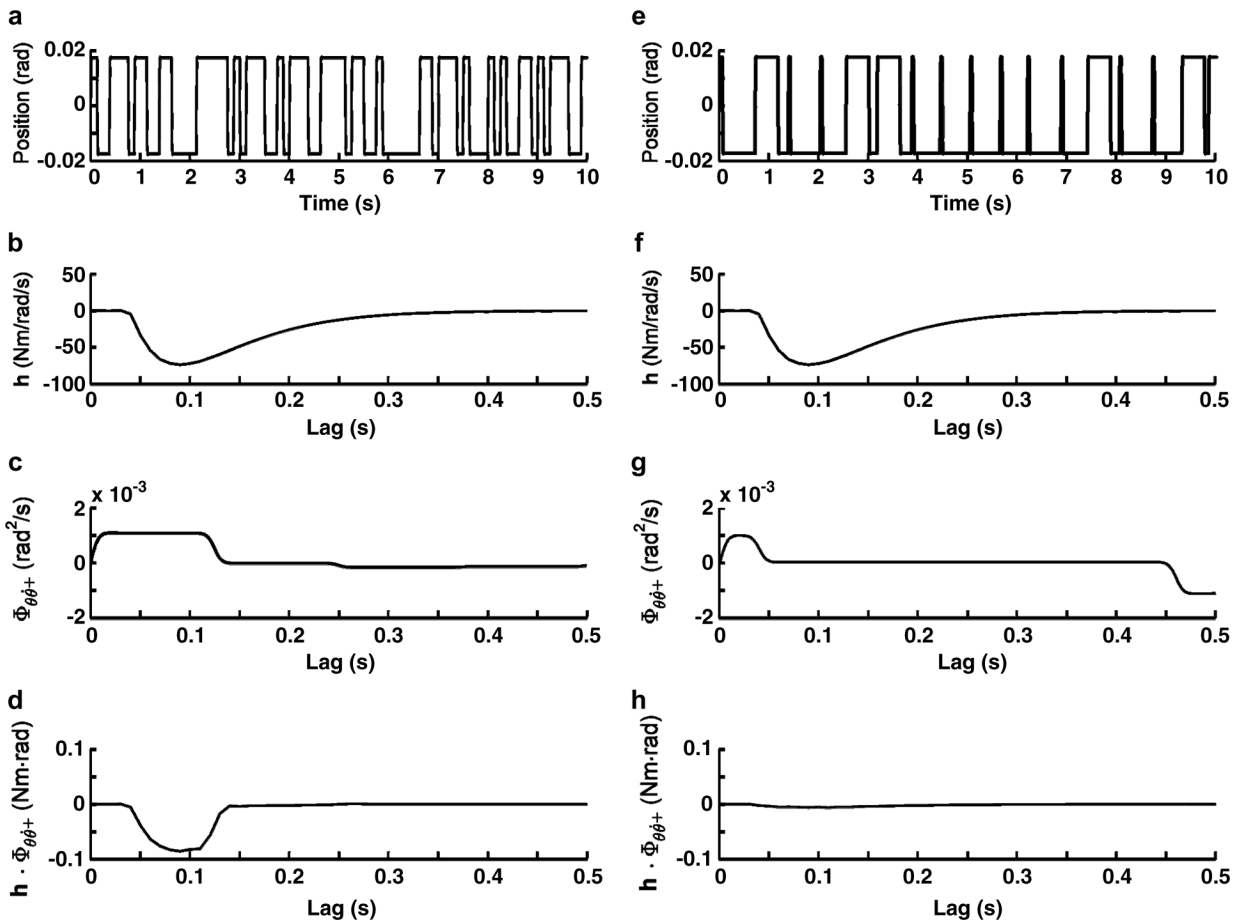

Fig. 2. (a) Position, (b) reflex stiffness IRF ($\mathbf{h}$), (c) $\Phi_{\theta\dot{\theta}+}$, (d) product of $\mathbf{h}$ and $\Phi_{\theta\dot{\theta}+}$ for a PRBS input signal with a 125 ms switching interval. (e) Position, (f) reflex stiffness IRF ($\mathbf{h}$), (g) $\Phi_{\theta\dot{\theta}+}$, (h) product of $\mathbf{h}$ and $\Phi_{\theta\dot{\theta}+}$ for a "pulse-step" input signal. Since $\mathbf{h}$ is nonzero from 40–400 ms and $\Phi_{\theta\dot{\theta}+}$ for the PRBS is nonzero from 0–125 ms, the product is nonzero from 40–125 ms. The $\Phi_{\theta\dot{\theta}+}$ for the "pulse-step" input signal is zero from 40–400 ms, resulting in a product which is zero at all times.

levels of mean ankle velocity suppress the reflex response [6]. Thus, at a switching rate of 40 ms, which has a high average velocity, there would be no reflex response.

Therefore, we sought a novel perturbation sequence whose properties would eliminate the reflex contributions from (2). This perturbation must:

1) have an average velocity low enough to preserve the stretch reflex response;
2) have $\Phi_{\theta\dot{\theta}+}$ equal to zero for lags between 40 and 400 ms.

This was accomplished by designing an input sequence that switches randomly between 500 ms "pulse" and "step" segments [Fig. 2(e)]. "Pulses" consisted of 40 ms pulses, while "steps" were 460 ms pulses. This results in a perturbation in which, during 40 ms to 460 ms after each dorsiflexing displacement, the position returns to the original position half the time and remains at the stretched position the other half of the time. Consequently, $\Phi_{\theta\dot{\theta}+}$ equals 0 from 40 ms to 460 ms [Fig. 2(g)]. Each segment was followed by a random pause lasting between 0 and 200 ms to make the perturbation unpredictable. Fig. 2(h) shows that the product of $\mathbf{h}$ and $\Phi_{\theta\dot{\theta}+}$ for this perturbation is negligible. Thus, the zero-lag cross-correlation between position and the reflex torque using the "pulse-step" perturbation will average to zero and (2) reduces to

$$E[\theta \bullet TQ] \approx E[\theta \bullet TQ_I]. \tag{8}$$

The second requirement was that the average velocity should be low. Ref. [14] showed that the stretch reflex response decreases with increasing average velocity. A "pulse-step" perturbation of 0.035 rad has an average absolute velocity of 0.12 rad/s while that of the 125 ms PRBS, with the same peak-to-peak amplitude, was 0.17 rad/s. Therefore, the "pulse-step" perturbation should suppress reflex less than the 125 ms PRBS.

B. Estimation of Intrinsic Stiffness

For small perturbations and a fixed operating point, a wide range of studies have shown that the intrinsic torque can be modeled well with three components, inertial, viscous, and elastic, that depend on the position of the ankle and its derivatives [1], [6], [9]. Thus, intrinsic stiffness may be modeled as

$$TQ_I = I\ddot{\theta} + B\dot{\theta} + K\theta \tag{9}$$

where θ is position and I, B, and K are the inertial, viscous, and elastic parameters, respectively. Hence, the cross-correlation between position and intrinsic torque is

$$E[\theta \bullet TQ] = IE[\theta \bullet \ddot{\theta}] + BE[\theta \bullet \dot{\theta}] + KE[\theta \bullet \theta]. \tag{10}$$

Since there are three unknowns, three equations are required to solve for the parameters. In addition to the cross-correlation

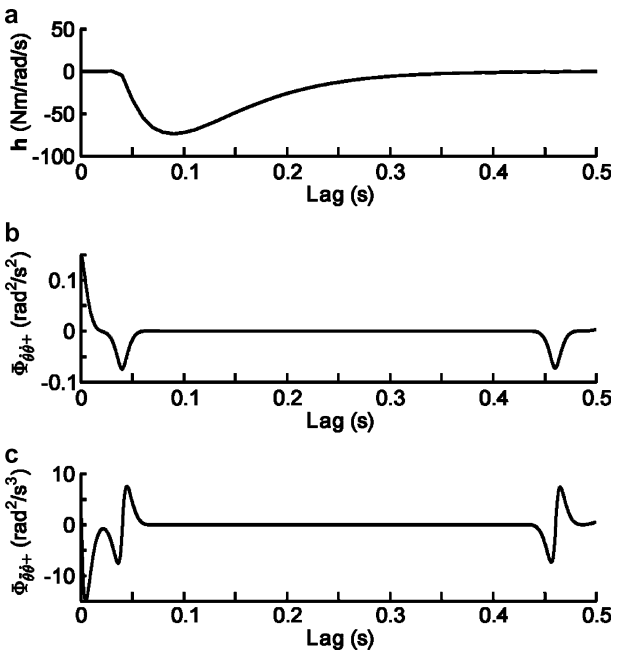

Fig. 3. (a) Reflex stiffness IRF ($\mathbf{h}$), (b) $\Phi_{\dot\theta\dot\theta+}$, and (c) $\Phi_{\ddot\theta\dot\theta+}$ for "pulse-step" input signal. Both $\Phi_{\dot\theta\dot\theta+}$ and $\Phi_{\ddot\theta\dot\theta+}$ are near zero when the $\mathbf{h}$ is nonzero.

between position and torque, we can form the cross-correlation between velocity and torque

$$E[\dot\theta \bullet TQ] = IE[\dot\theta \bullet \ddot\theta] + BE[\dot\theta \bullet \dot\theta] + KE[\dot\theta \bullet \theta] + E[\dot\theta \bullet TQ_R] \tag{11}$$

and between acceleration and torque

$$E[\ddot\theta \bullet TQ] = IE[\ddot\theta \bullet \ddot\theta] + BE[\ddot\theta \bullet \dot\theta] + KE[\ddot\theta \bullet \theta] + E[\ddot\theta \bullet TQ_R]. \tag{12}$$

As was done for the position, the cross-correlation between velocity and reflex torque, and acceleration and reflex torque can be estimated by looking at $\Phi_{\dot\theta\dot\theta+}$ and $\Phi_{\ddot\theta\dot\theta+}$ respectively (Fig. 3). Since $\Phi_{\dot\theta\dot\theta+}$ and $\Phi_{\ddot\theta\dot\theta+}$ are near zero when $\mathbf{h}$ is nonzero the cross-correlation between velocity and reflex torque, and acceleration and reflex torque are both approximately zero.

Combining (10), (11), and (12), and rewriting in matrix format gives

$$\begin{bmatrix} E[\theta \bullet Tq] \\ E[\dot\theta \bullet Tq] \\ E[\ddot\theta \bullet Tq] \end{bmatrix} = \begin{bmatrix} E[\theta \bullet \theta] & E[\theta \bullet \dot\theta] & E[\theta \bullet \ddot\theta] \\ E[\dot\theta \bullet \theta] & E[\dot\theta \bullet \dot\theta] & E[\dot\theta \bullet \ddot\theta] \\ E[\ddot\theta \bullet \theta] & E[\ddot\theta \bullet \dot\theta] & E[\ddot\theta \bullet \ddot\theta] \end{bmatrix} \begin{bmatrix} K \\ B \\ I \end{bmatrix}. \tag{13}$$

Solving (13) gives estimates for K, B, and I.

C. Estimation of Reflex Stiffness

Once the estimates from (13) are known, the reflex torque can be estimated as

$$\hat{TQ}_R = TQ - \hat I\ddot\theta - \hat B\dot\theta - \hat K\theta. \tag{14}$$

Reflex stiffness at the ankle has been modeled as a delay and a uni-directional rate-sensitive element followed by linear dynamics. The dynamics may be second or third order depending on the subject and operating point. Consequently, we felt it best to estimate the dynamics nonparametrically using an IRF.

Thus, the reflex torque was modeled as (15), shown at the bottom of the page, where $\dot\theta^+$ is half-wave rectified velocity, m is the number of lags, and n is the length of the signals. Solving (15) for $\mathbf{h}$ will estimate the reflex stiffness IRF. The gain of the reflex stiffness (G) can then be found by integrating $\mathbf{h}$.

D. Implementation

The real-time estimation algorithm, shown in Fig. 4, was implemented using Simulink (The Mathworks Inc.) for simulation data, and xPC Target (The Mathworks Inc.) for experimental data. In both cases, the estimation algorithm ran at a fixed rate of 1 kHz. The following steps, which outline the estimation procedure, were carried out at every sample time.

1) The torque was high-pass filtered at 0.033 Hz.
2) The products in the matrices in (13) were formed and low-pass filtered.
3) K, B, and I were estimated by solving (13) with an LDL solver, which factors the matrix into a lower triangular matrix, a diagonal matrix, and the Hermitian transpose of the lower triangular matrix.
4) $\hat{TQ}_R$ was estimated from (14) and then high-pass filtered.
5) The position signal was differentiated, half-wave rectified, and high-pass filtered at 0.033 Hz, to give a zero-mean half-wave rectified velocity signal $\dot\theta^+$.
6) $\hat{TQ}_R$ and $\dot\theta^+$ were filtered with an eighth order type-1 low-pass Chebyshev, with a cutoff of 40 Hz and passband ripple of 0.05 dB, and then downsampled to 100 Hz.
7) Equation (15) was formed by concatenating lagged $\dot\theta^+$ signals. Each lag was 10 ms with the minimum lag being 50 ms and the max lag being 400 ms.
8) The reflex stiffness IRF ($\hat{\mathbf{h}}$) was estimated by finding the least-squares solution to (15) using a QR solver, with a 1 s data length, every 100 ms. This gives a nonparametric estimate of the reflex stiffness.
9) Reflex stiffness gain was estimated by summing $\hat{\mathbf{h}}$.

E. Validation

The parallel-cascade identification algorithm was used to validate the estimates produced by the real-time estimation algo-

$$\begin{bmatrix} \hat{TQ}_R(j\Delta t) \\ \hat{TQ}_R((j-1)\Delta t) \\ \vdots \\ \hat{TQ}_R((j-n)\Delta t) \end{bmatrix} = \begin{bmatrix} \dot\theta^+(j\Delta t) & \dot\theta^+((j-1)\Delta t) & \dots & \dot\theta^+((j-m)\Delta t) \\ \dot\theta^+((j-1)\Delta t) & \dot\theta^+((j-2)\Delta t) & \dots & \dot\theta^+((j-1-m)\Delta t) \\ \vdots & \vdots & \ddots & \vdots \\ \dot\theta^+((j-n)\Delta t) & \dot\theta^+((j-n-1)\Delta t) & \dots & \dot\theta^+((j-n-m)\Delta t) \end{bmatrix} \begin{bmatrix} h(0) \\ h(1) \\ \vdots \\ h(m) \end{bmatrix} \tag{15}$$

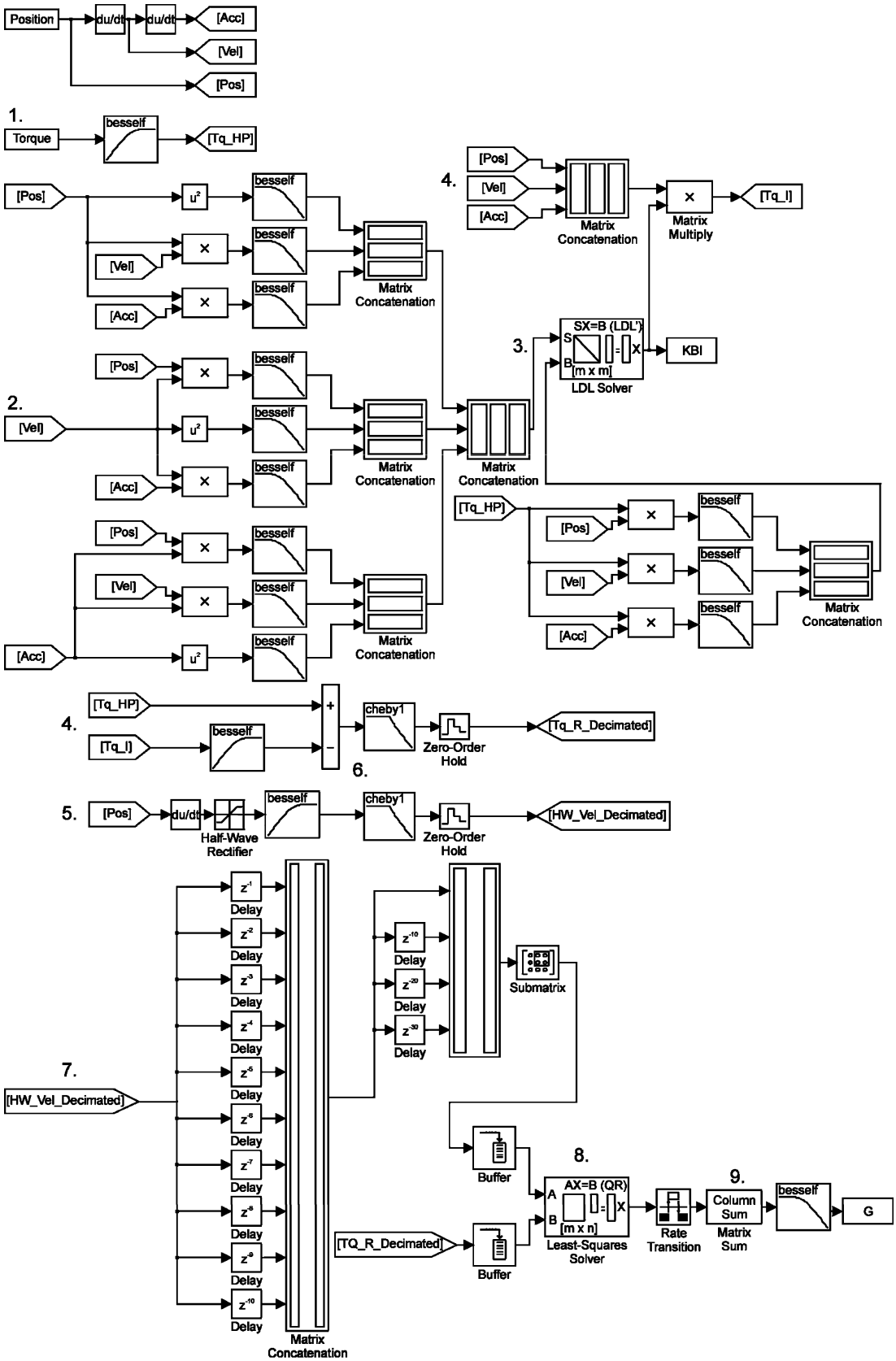

Fig. 4. Simulink model of the real-time estimation algorithm. Numbers correspond to the steps described in Section II-D.

rithm. This analysis was performed off-line using the entire length of data after the experimental or simulation run. This parallel-cascade identification algorithm was described previously in [6] and will be described only briefly here.

1) Intrinsic stiffness was estimated by finding the IRF between the position and torque. The maximum lag of the IRF was set to 40 ms, preventing any contribution from the reflex torque.

2) Reflex torque was estimated by subtracting the predicted intrinsic torque from the net torque.
3) Reflex stiffness was estimated by finding the IRF between half-wave rectified velocity and the estimated reflex torque.
4) The intrinsic torque was re-estimated by subtracting the predicted reflex torque from the net torque.
5) The intrinsic stiffness was re-estimated by finding the IRF between the position and the estimated intrinsic torque.
6) The procedure was repeated until the percentage of variance accounted for (%VAF) of the total predicted torque ceased to increase.

III. Simulation Studies

A. Simulation Model

Simulations were carried out to test the accuracy, precision, and response time of the real-time estimation algorithm. Reflex and intrinsic torques were simulated based on the parallel-cascade model of ankle stiffness (Fig. 1) using Simulink. Intrinsic torque was simulated by multiplying the position, the velocity, and the acceleration by the elastic, viscous, and inertial stiffness, respectively. Reflex torque was simulated by applying a half-wave rectifier to the delayed velocity and then convolving it with a second order low-pass system. Previous studies found that the reflex stiffness dynamic can be modeled as either a second or third order system depending on the subject and the operating point. For the purpose of these simulations, we used only a second order low-pass system defined in the Laplace domain as

$$\frac{TQ_R(s)}{\dot{\theta}^+(s)} = \frac{Gw^2}{s^2 + 2zws + w^2}. \tag{16}$$

Independent white noise was added to the position to give an input signal-to-noise ratio (SNR) of 70 dB, and to the torque to give an output SNR of 40 dB, emulating the noise levels expected during experimental trials.

B. Simulation Methods

Each simulation ran for 240 s with a 1 ms increment. The first 30 s of real-time estimates were ignored to avoid errors due to simulation transients. The elastic stiffness (K) and the reflex stiffness gain (G) are the parameters that vary most in physiological situations [7]; thus, our analysis focused on these. Three sets of simulations were performed to assess the accuracy, variability, and response time of the algorithm. The following section explains these simulations in detail.

C. Simulation Results

1) Accuracy: One hundred simulation runs were done for each of the following conditions.

1) K was chosen randomly from 0–200 Nm/rad while G was held constant at 10 Nm/rad/s.
2) G was chosen randomly from 0–20 Nm/rad/s while K was held constant at 100 Nm/rad.
3) Both K and G were chosen independently and randomly from 0–200 Nm/rad and 0–20 Nm/rad/s, respectively.

All other parameters were held constant with values that resemble those found in previous experiments (B = 0.63 Nm/rad/s, $I = 0.0137$ Nm/rad/s^2, $w = 21$ rad/s, $z = 0.8$) [6], [7]. The accuracies of the estimates were compared by calculating the %VAF

$$\%\text{VAF} = \left[1 - \frac{\text{var}(\hat{\mathbf{x}} - \mathbf{x})}{\text{var}(\mathbf{x})}\right] \times 100\% \tag{17}$$

where $\mathbf{x}$ is the set of simulated parameter values from all simulation runs and $\hat{\mathbf{x}}$ is the corresponding set of estimated parameters.

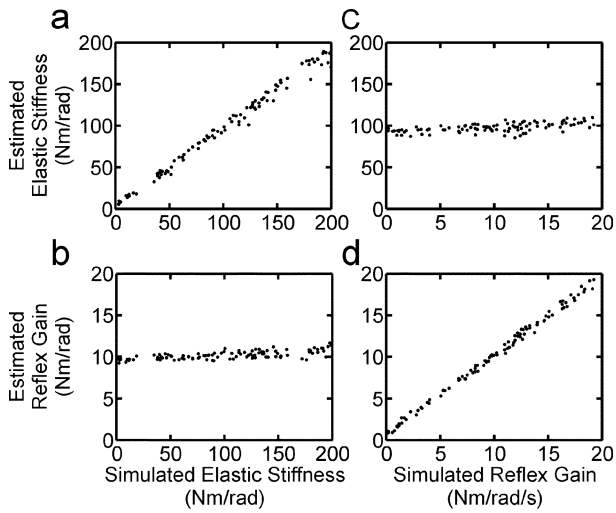

Fig. 5. Estimation of (a) elastic stiffness and (b) reflex gain when K was varied randomly from 0–200 Nm/rad and G was held constant at 10 Nm/rad/s. Estimation of (c) elastic stiffness and (d) reflex gain when G was varied randomly from 0–20 Nm/rad/s and K held constant at 100 Nm/rad. Each point corresponds to a separate simulation and represents the mean of the parameter estimate for that simulation.

Fig. 5(a) and (b) show the estimates of K and G for runs where K was chosen randomly between 0 and 200 Nm/rad while G was held constant at 10 Nm/rad/s. Each point corresponds to a separate simulation run and represents the time average of the estimated parameter. The estimates of K were close to the simulated values for all runs [Fig. 5(a), %VAF = 98.6%] while the estimates of G [Fig. 5(b)] were almost constant $(G = 10.2 \pm 0.5$ Nm/rad/s).

Fig. 5(c) and (d) show the results of the converse experiment, where G was selected to be between 0 and 20 Nm/rad/s while K was held constant at 100 Nm/rad. The estimates of G were close to the simulated values [Fig. 5(d), %VAF = 99.3%], while those of K remained almost constant [Fig. 5(c), $K = 98 \pm 5$ Nm/rad].

Though not shown, the algorithm also estimated the values of B and I—when K and G were varied simultaneously—to be 0.63 ± 0.03 Nm/rad/s and 0.0137 ± 0.0002 Nm/rad/s^2, respectively, matching the simulated values of 0.63 Nm/rad/s and 0.0137 Nm/rad/s^2. Furthermore, the estimates of B and I did not covary with elastic stiffness or reflex gain as evident by their low standard deviations.

The real-time estimation algorithm was also compared to the parallel-cascade algorithm on a subset of 20 simulations in which K and G both varied. Fig. 6 shows that both the parallel-cascade and real-time estimates closely matched the ideal line. Thus, the real-time estimation performed almost as well as the parallel-cascade identification in estimating both K and G.

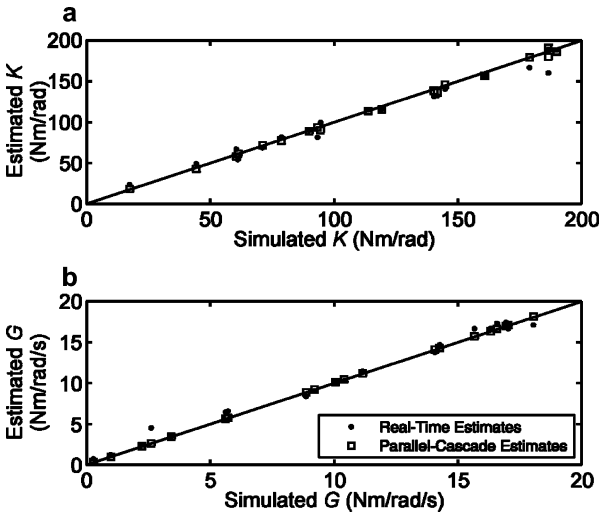

Fig. 6. Real-time and parallel-cascade estimates of elastic stiffness and reflex gain. Both methods of estimation performed very well in identifying (a) elastic stiffness and (b) reflex gain, when both K and G were varied simultaneously.

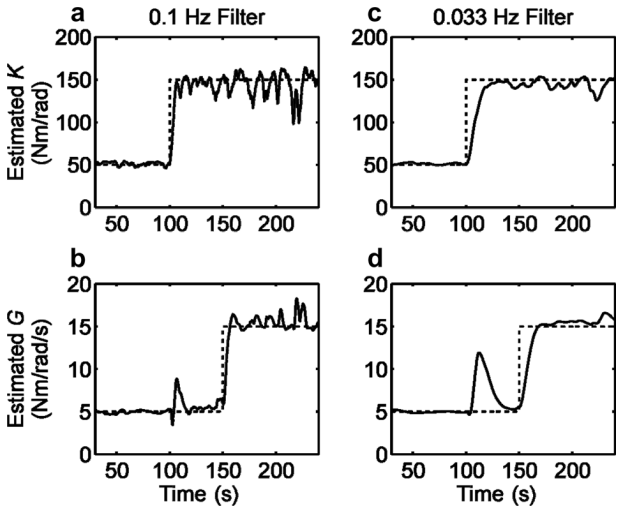

Fig. 7. Response time of real-time estimates. Position and torque were simulated with step changes in elastic stiffness and reflex gain occurring at 100 s and 150 s, respectively. Using the 0.1 Hz filter (left) the response time is much quicker for both (a) elastic stiffness and (b) reflex gain than the response time for the (c) elastic stiffness and (d) reflex gain estimates produced by the 0.033 Hz filter (right).

2) Variability: Next we examined the variance of the real-time estimates. Reflex and intrinsic torque were simulated once with $K = 100$ Nm/rad and $G = 10$ Nm/rad/s, and all other parameters as before. The variance in time of the estimates was estimated from 30 s until the end.

A low-pass filter was used to perform the averaging in (9), as well as averaging the reflex stiffness gain estimate. In selecting this filter there is a tradeoff between variance, which will decrease with the filter cut-off, and response time. Filters at two different cut-off frequencies were tested, one at 0.1 Hz and the other at 0.033 Hz. When a 0.1 Hz low-pass filter was used to perform the averaging, the standard deviation was 11.9% of the mean for K and 7.2% for G. With a 0.033 Hz low-pass filter, the standard deviations dropped to 7.9% and 5.2% for K and G, respectively. The lower standard deviations of the 0.033 Hz low-pass filter show that this filter provides estimates with less variance. However, the increased averaging will also increase the response time.

3) Response Time: Finally we examined the response time of the estimation algorithm. Simulations were run in which K and G underwent step changes at different times. The risetime, defined as the time taken for the parameter estimates to go from 10% to 90% of its change, was calculated for both parameters.

Fig. 7 shows the time course of the K and G estimates using the two filters following step changes in the simulated parameter values. The dotted lines in each figure show the simulated parameter values, while the solid lines show the estimates. Using the 0.1 Hz filter, the risetime for K was 4.6 s [Fig. 7(a)] and 4.6 s for G [Fig. 7(b)]. Using the 0.033 Hz filter, the risetimes for K and G were 14.2 s and 11.9 s, respectively [Fig. 7(c), (d)]. Thus, increased averaging reduces parameter variance but makes the estimation algorithm respond more slowly.

In addition to the step change in the reflex gain estimate that occurred at 150 s, there was another change at 100 s. This is due to the change in elastic stiffness. When the elastic stiffness changes, the reflex torque estimate will be biased until the elastic stiffness estimate reaches its true value. This bias will lead to a bias in the reflex stiffness as evident by the displacement seen in the reflex gain trace. Thus, when intrinsic stiffness is changing and reflex stiffness remains constant, we must wait for the transients to subside before obtaining reliable reflex stiffness estimates. Therefore, a limitation of the algorithm is that reflex stiffness cannot be estimated when intrinsic stiffness varies. However, the reverse does not apply; because intrinsic stiffness is estimated prior to estimating reflex stiffness, changes in reflex stiffness do not bias intrinsic stiffness estimates.

IV. Experimental Results

We further validated the algorithm using experimental data and comparing the real-time estimates to those of the off-line parallel-cascade algorithm. To achieve this, experiments were conducted in which the position and torque were recorded in addition to the real-time estimates.

A. Experimental Methods

1) Apparatus: Subjects lay supine with the left foot attached to an electrohydraulic actuator by a custom-made fiberglass boot. Movement of the foot was restricted to plantarflexion and dorsiflexion. The left leg was immobilized with a leather strap and supported with two sand bags under the knee. Two safety stops, one physical and one hydraulic, limited the actuator movement to the subjects' voluntary range of motion.

Subjects' ankle position was measured with a potentiometer (BI Technologies 6273), and torque with a torque transducer (Lebow 2110-5K). Both position and torque were defined to be positive for dorsiflexion and negative for plantarflexion.

Position and torque were sampled at 1 kHz using an NI-4472 data acquisition card. Anti-aliasing was performed by the card which over-sampled the data and then applied a digital brick-wall filter with a 486.3 Hz cutoff frequency. Data were then stored on the Host PC (AMD Athlon 1.33 GHz, 1 GB RAM).

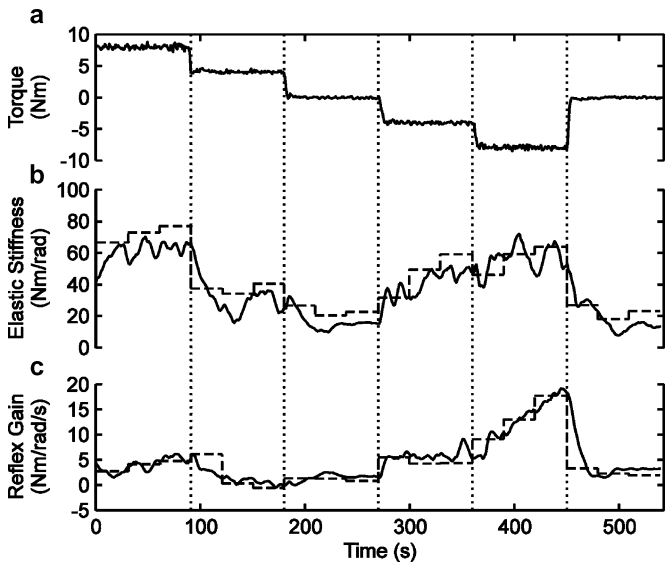

Fig. 8. Real-time and parallel-cascade estimates of reflex gain and elastic stiffness in experimental data. Real-time estimates (solid line) were collected in an experimental trial where the subject varied her (a) torque at 90 s intervals. Parallel-cascade estimates (dashed line) were generated for 30 s intervals following experiment using recorded position and torque values. Parallel-cascade estimates for (b) elastic stiffness and (c) reflex gain closely matched real-time estimates.

The controller and the real-time identification were implemented using xPC Target on the Target PC (AMD Athlon 1.6 GHz, 256 MB RAM). Position and torque were sampled on this machine for actuator control and real-time identification of intrinsic stiffness and reflex gain. Sampling was done at 1 kHz using a ComputerBoards PCIM-DAS1602/16 Analog-to-Digital Card. Prior to sampling, data were filtered with 8-pole, 6-zero, linear phase, constant delay, low-pass filter with a cutoff of 400 Hz (Frequency Devices 9064). The control signal was output with a ComputerBoards PCIM-DDA06/16 Digital-to-Analog Card to the servo-valve which controlled the position of the actuator.

Visual feedback was generated using a display which was custom-built using Simulink on the Display PC (Intel Pentium III 500 MHz, 256 MB RAM). Feedback data was calculated on Target PC and sent to display PC via the UDP network protocol. Feedback was displayed on a 15-inch LCD monitor (NEC) mounted over the subjects' heads.

2) Procedure: The experimental paradigm was a simple torque matching task, since it is known that both elastic stiffness and reflex stiffness gain vary with torque levels [7]. Subjects were provided with a display of their average torque on the LCD monitor and were asked to maintain it at a fixed level. The torque target began at 8 Nm, and decreased by 4 Nm every 90 s, until the completion of a 90 s interval at -8 Nm, at which point the target returned to zero [see Fig. 8(a)].

All experiments were done with the low-pass filters at 0.033 Hz because subjects were most comfortable controlling joint stiffness with the increased averaging.

B. Experimental Results

Fig. 8(a) shows the mean torque and the real-time and parallel-cascade estimates for elastic stiffness [Fig. 8(b)] and reflex gain [Fig. 8(c)] recorded during an experimental trial. Parallel-cascade estimates were generated using 30 s worth of data. As mentioned previously, the risetime for the elastic stiffness was 14.2 s with 0.033 Hz filter, so the real-time estimates for at least the first 15 s of each interval should be ignored. For both elastic stiffness and reflex stiffness gain, the mean of the real-time estimates for each interval closely matched the parallel-cascade estimates for that interval (%VAF $= 90\%$ for both K and G). The real-time and parallel-cascade estimates of K covaried, as evident by the high %VAF, but there appears to be an offset between these two estimates.

V. Discussion

We have shown that using the "pulse-step" position input, intrinsic and reflex stiffness can be separated and estimated in real time. Intrinsic stiffness was estimated by finding the cross-correlation between the position, its derivatives, and the torque. Reflex stiffness gain was estimated by finding the IRF between a delayed half-wave rectified velocity signal and the torque. Using simulated data, it was found that the real-time algorithm estimated the parameter values accurately. Using two different filters to perform averaging, it was found that the algorithm could either produce estimates with low variance and slow response times or high variance and quick response times. Validation of the real-time estimates with the parallel-cascade identification algorithm demonstrated that both estimates were in agreement for both simulated and experimental data.

It has been shown previously that reflex and intrinsic stiffness can be separated using off-line analysis methods [6]. Here we show for the first time that the two components can be estimated accurately in real time. The key to the estimation was the use of the "pulse-step" position input which was designed specifically to eliminate the covariance of two stiffness estimates. For this perturbation, $\Phi_{\theta\dot{\theta}+}$ is equal to zero for lags between 40 and 460 ms, consequently the zero-lag cross-correlation between position and reflex torque equals zero. Furthermore, both $\Phi_{\dot{\theta}\dot{\theta}+}$ and $\Phi_{\ddot{\theta}\dot{\theta}+}$ are zero when $\mathbf{h}$ is nonzero, resulting in both the product of velocity and reflex torque and acceleration and reflex torque equaling zero. Using the products of the torque with the position and its derivatives, the three components of the intrinsic stiffness were found by solving a system of three linear equations. While only one component—the elastic stiffness—was shown to be identified successfully over a large range of values, the other two components were identified just as successfully for static values. However, since these other components change only slightly [7], there is little interest in investigating their behavior in real time.

Reflex stiffness has been modeled as a second—and sometimes third—order low-pass system with a delay [6]. We estimated reflex stiffness nonparametrically by calculating the IRF between half-wave rectified velocity and the estimated reflex torque. We then determined the gain of the reflex stiffness by integrating the resultant IRF. Since the gain of the reflex stiffness is the most variable parameter [7], this was the only parameter calculated. While it is possible to fit a second or third order model to the IRF to determine the other parameters of the reflex stiffness, this would require us to make an assumption about the structure of the reflex stiffness. Therefore, we felt it better to simply integrate the IRF to calculate the gain.

A. Limitations of the Real-Time Algorithm

The real-time estimation algorithm performs very well in simulations, but has some limitations. The real-time estimation depends on the averaging of two values which are randomly distributed to remove the reflex torque from the total torque. Given enough data there would be equal amounts of each value to ensure that expectation value is zero. However, since the task is to produce a real-time estimate, the data length must be restricted so that the algorithm produces estimates that reflect current and not past values. Thus, at any given time there may be a slight bias in the estimates due to the uneven distribution of "pulses" and "steps".

The real-time algorithm is also limited to measuring intrinsic and reflex stiffness in steady-state conditions. Voluntary torque is removed under the assumption that it remains constant. Therefore, when voluntary torque is not constant both reflex and intrinsic stiffness estimates may be biased. Furthermore, due to the need for averaging, the estimates can only be considered accurate 15 s after the voluntary torque stops changing.

A similar limitation occurs during changes of intrinsic stiffness. Due to the averaging, the intrinsic torque may be inaccurate for the first 15 s following a change in intrinsic stiffness. Since reflex torque is estimated by subtracting intrinsic torque from net torque, it too may be inaccurate for the 15 s following changes in intrinsic stiffness, even when torque remains constant. Thus, the algorithm tracks changes but its estimates can only be relied upon once conditions stabilize.

Finally, we observed an offset between the parallel-cascade and real-time estimates when experimental data was used. This offset was not present for simulated data, thus we are unsure of its origins. We suspect that the offset may arise due to differences in estimating intrinsic stiffness between the parallel-cascade and real-time algorithms. For the purpose of using the estimates as feedback, the offset is not very important provided that the variations reflect the variations of the underlying parameters. Since the parallel-cascade and real-time estimates covaried, we are confident that the variations of the real-time estimates reflect the variations of the underlying parameters.

B. Applications of the Real-Time Algorithm

We foresee that the main application of the real-time algorithm will be to provide feedback for subjects. We have used an earlier, simpler version of this real-time estimation algorithm [15] to estimate elastic stiffness and reflex gain in real time and use it as feedback. We found that subjects, given proper feedback, could vary their reflex stiffness gain by a factor of 4, while maintaining elastic stiffness and background torque constant. Further experiments showed that subjects could change their reflexes rapidly on command. These experiments demonstrated that subjects can control reflex stiffness independently and so have great flexibility in adjusting the mechanical properties of their joints to meet functional requirements.

There are a number of medical conditions, such as traumatic brain injury, stroke, and spinal cord injury, that can lead to spasticity, resulting in exaggerated stretch reflexes and a general increase in muscle tone [16]. Using the parallel-cascade algorithm, it has been shown that spinal cord injuries increase intrinsic stiffness slightly and reflex stiffness greatly [16], while strokes cause an increase reflex stiffness in some subjects but no change in intrinsic stiffness [17]. Ref. [16] found that the intrinsic stiffness was still well modeled by (9), while the reflex stiffness IRF in spinal cord injured patients was nonzero from 40 to 600 ms. Thus, our real-time algorithm could successfully work with spinal cord injured patients, with a slight modification in the perturbation sequence so that $\Phi_{\theta\dot{\theta}+}$ is zero from 40 to 600 ms. Ref. [17] found that, in stroke patients, intrinsic stiffness was well modeled by (9), and reflex stiffness was nonzero between 40 and 300 ms, satisfying the requirements needed for the real-time algorithm. Currently, clinical stiffness measurements are performed by hand or using hand-held dynamometers [18], [19]. The real-time estimation algorithm would allow clinicians to easily quantify the reflex and intrinsic stiffness in real time and assess the degree of spasticity. Furthermore, real-time estimates of reflex stiffness could be used as feedback for helping patients treat their spasticity, similar to what was done in [20]–[23].

REFERENCES

[1] R. E. Kearney and I. W. Hunter, "System identification of human joint dynamics," *Crit. Rev. Biomed. Eng.*, vol. 18, pp. 55–87, 1990.

[2] T. R. Nichols and J. C. Houk, "Improvement in linearity and regulation of stiffness that results from actions of stretch reflex," *J. Neurophysiol.*, vol. 39, pp. 119–142, 1976.

[3] J. Noth, H. R. Matthews, and H. H. Friedemann, "Long latency reflex force of human finger muscles in response to imposed sinusoidal movements," *Exp. Brain Res.*, vol. 55, pp. 317–324, 1984.

[4] R. R. Carter, P. E. Crago, and M. W. Keith, "Stiffness regulation by reflex action in the normal human hand," *J. Neurophysiol.*, vol. 64, pp. 105–118, 1990.

[5] T. Sinkjaer, E. Toft, S. Andreassen, and B. C. Hornemann, "Muscle stiffness in human ankle dorsiflexors: Intrinsic and reflex components," *J. Neurophysiol.*, vol. 60, pp. 1110–1121, 1988.

[6] R. E. Kearney, R. B. Stein, and L. Parameswaran, "Identification of intrinsic and reflex contributions to human ankle stiffness dynamics," *IEEE Trans. Biomed. Eng.*, vol. 44, no. 6, pp. 493–504, Jun. 1997.

[7] M. M. Mirbagheri, H. Barbeau, and R. E. Kearney, "Intrinsic and reflex contributions to human ankle stiffness: Variation with activation level and position," *Exp. Brain Res.*, vol. 135, pp. 423–436, 2000.

[8] D. Ludvig, M. Baker, I. Cathers, and R. E. Kearney, "Task-dependence of ankle stretch reflex," in . *Proc. 25th Annu. Int. Conf. IEEE Engineering in Medicine and Biology Soc. (EMBS) 2003*, Cancun, Mexico, Sep. 2003, pp. 1487–1490.

[9] L. Q. Zhang and W. Z. Rymer, "Simultaneous and nonlinear identification of mechanical and reflex properties of human elbow joint muscles," *IEEE Trans. Biomed. Eng.*, vol. 44, no. 12, pp. 1192–1209, Dec. 1997.

[10] J. F. Lehmann, R. Price, B. J. deLateur, S. Hinderer, and C. Traynor, "Spasticity: Quantitative measurements as a basis for assessing effectiveness of therapeutic intervention," *Arch. Phys. Med. Rehabil.*, vol. 70, pp. 6–15, 1989.

[11] M. Meinders, R. Price, J. F. Lehmann, and K. A. Questad, "The stretch reflex response in the normal and spastic ankle: Effect of ankle position," *Arch. Phys. Med. Rehabil.*, vol. 77, pp. 487–492, 1996.

[12] J. C. Houk, "An assessment of stretch reflex function," *Prog. Brain Res.*, vol. 44, pp. 303–314, 1976.

[13] D. Ludvig and R. E. Kearney, "Real-time estimation of intrinsic and reflex stiffness," in *Proc. 28th Annu. Int. Conf. IEEE Engineering in Medicine and Biology Soc. (EMBS) 2006*, New York, Aug. 2006, pp. 292–295.

[14] R. B. Stein and R. E. Kearney, "Nonlinear behavior of muscle reflexes at the human ankle joint," *J. Neurophysiol.*, vol. 73, pp. 65–72, 1995.

[15] D. Ludvig, I. Cathers, and R. E. Kearney, "Voluntary modulation of human stretch reflexes," *Exp. Brain Res.*, in press.

[16] M. M. Mirbagheri, H. Barbeau, M. Ladouceur, and R. E. Kearney, "Intrinsic and reflex stiffness in normal and spastic, spinal cord injured subjects," *Exp. Brain Res.*, vol. 141, pp. 446–459, 2001.

[17] L. Galiana, J. Fung, and R. Kearney, "Identification of intrinsic and reflex ankle stiffness components in stroke patients," *Exp. Brain Res.*, vol. 165, pp. 422–434, 2005.

[18] A. Lamontagne, F. Malouin, C. L. Richards, and F. Dumas, "Evaluation of reflex- and nonreflex-induced muscle resistance to stretch in adults with spinal cord injury using hand-held and isokinetic dynamometry," *Phys. Ther.*, vol. 78, pp. 964–975, 1998, discussion 976-8.

[19] B. Ashworth, "Preliminary trial of carisoprodol in multiple sclerosis," *Practitioner*, vol. 192, pp. 540–542, 1964.
[20] M. L. Evatt, S. L. Wolf, and R. L. Segal, "Modification of human spinal stretch reflexes: Preliminary studies," *Neurosci. Lett.*, vol. 105, pp. 350–355, 1989.
[21] R. L. Segal and S. L. Wolf, "Operant conditioning of spinal stretch reflexes in patients with spinal cord injuries," *Exp. Neurol.*, vol. 130, pp. 202–213, 1994.
[22] S. L. Wolf and R. L. Segal, "Conditioning of the spinal stretch reflex: Implications for rehabilitation," *Phys. Ther.*, vol. 70, pp. 652–656, 1990.
[23] S. L. Wolf and R. L. Segal, "Reducing human biceps brachii spinal stretch reflex magnitude," *J. Neurophysiol.*, vol. 75, pp. 1637–1646, 1996.

Daniel Ludvig (S'06) was born in 1981 in Montreal, QC, Canada. He received the B.Sc. degree in physiology and physics in 2003 and the M.Eng. degree in biomedical engineering in 2006 from McGill University, Montreal, QC. He is currently pursuing the Ph.D. degree in biomedical engineering at McGill University.

His research interests include the human stretch reflex and identification of physiological systems.

Robert E. Kearney (M'76–SM'92–F'01) received the Ph.D. degree in mechanical engineering from McGill University, Montreal, QC, Canada, in 1976.

He is a Professor in the Department of Biomedical Engineering, Faculty of Medicine at McGill University. He maintains an active research program that focuses on using quantitative engineering techniques to address biomedical research problems. Specific areas of his research include: the development of algorithms and tools for biomedical system identification; the application of system identification to understand the role played by stretch reflexes and joint mechanics in the control of posture and movement; and the development of bioinformatics tools and techniques for proteomics.

Dr. Kearney is a Fellow of the IEEE, the Engineering Institute of Canada, and the American Institute of Medical and Biological Engineering, and is a recipient of the IEEE Millennium Medal.